

Hit2Flux: A Machine Learning Framework for Boiling Heat Flux Prediction Using Hit-Based Acoustic Emission Sensing

Christy Dunlap, Changgen Li, Hari Pandey, and Han Hu ¹

Department of Mechanical Engineering, University of Arkansas, Fayetteville, AR 72701 USA

Abstract:

This paper presents Hit2Flux, a machine learning framework for boiling heat flux prediction using acoustic emission (AE) hits generated through threshold-based transient sampling. Unlike continuously sampled data, AE hits are recorded when the signal exceeds a predefined threshold and are thus discontinuous in nature. Meanwhile, each hit represents a waveform at a high sampling frequency (~ 1 MHz). In order to capture the features of both the high-frequency waveforms and the temporal distribution of hits, Hit2Flux involves i) feature extraction by transforming AE hits into the frequency domain and organizing these spectra into sequences using a rolling window to form “sequences-of-sequences,” and ii) heat flux prediction using a long short-term memory (LSTM) network with sequences of sequences. The model is trained on AE hits recorded during pool boiling experiments using an AE sensor attached to the boiling chamber. Continuously sampled acoustic data using a hydrophone were also collected as a reference data set for this study. Results demonstrate that the proposed AE-based method achieves performance comparable to hydrophones, validating its potential for heat flux monitoring. Additionally, it is shown that the inclusion of multiple acoustic emission hits as model inputs leads to higher performance. The Hit2Flux model is also compared to method pairing various signal preparation techniques with state-of-the-art models. This comparison further highlighted the superior accuracy of the proposed approach. The developed Hit2Flux algorithm can be applied to other transient sampling events, such as structural health monitoring, and detection of electromagnetic pulses, among others.

Keywords: Acoustics emission, Acoustic Hits Sequence, Boiling monitoring, Heat flux, Long short-term memory (LSTM) network.

1. INTRODUCTION

Thermal management is becoming a bottleneck in several industries such as high-power density electronics[1], electric vehicles[2], data centers [3], etc. Traditional single-phase methods are insufficient to meet the high-efficiency cooling demands of high-energy-density devices. Due to their high latent heat, two-phase methods have emerged as an alternative solution for advanced cooling systems and are in some cases implemented (e.g. immersion cooling of data centers [4]). As a representative method of two-phase

¹ Corresponding author. E-mail: hanhu@uark.edu (H. Hu),

Nomenclature

<i>Abbreviations</i>		l	Number of neurons
AE	Acoustic Emission	m	Amount of hits in an experiment
CNN	Convolutional Neural Network	n	Number of thermocouples
CHF	Critical Heat Flux	N	Sequence length
FFT	Fast Fourier Transform	p	Number of specified units
GPR	Gaussian Process Regression	q	Heat flux
HDT	Hit Definition Time	σ	Activation function
LSTM	Long Short-Term Memory	T_i	Temperature
MLP	Multilayer Perceptron	t'_i	Time relative to thermocouple
MSE	Mean Squared Error	$t_{i,1}$	Time of H_i start
RFR	Random Forest Regression	$t_{i,wl}$	Time at end of H_i
<i>Symbols</i>		Wl	Length of AE waveform
A	Total amount of sequences	z_i	Thermocouple position
C	LSTM cell state	L_{HP}	Length of hydrophone spectrum
Fl	Length of AE waveform spectrum	R^2	Coefficient of performance
f_i	LSTM forget gate	α	Stride
h	LSTM cell output	W	Weight matrix
H_i	AE Hit recorded waveform	b	Bias vector
H'_t	Frequency intensity of Hi	L_{MAE}	Loss function
i_i	LSTM input gate	n	Number of thermocouples
k	Thermal conductivity	N	Sequence length

heat dissipation, pool boiling has shown to be highly effective, as it operates with a high heat flux while maintaining a relatively low superheat in the nucleate boiling regime. However, there are several drawbacks when considering the feasibility of utilizing boiling for cooling. Boiling is a complex phenomenon involving intricate interactions among heat transfer, fluid dynamics, and phase change. Variations in surface conditions, fluid properties, and heat flux can lead to unpredictable safety issues, such as localized dry-out or boiling hysteresis. Additionally, there are instabilities associated with boiling that can have detrimental impacts on cooling.

One important instability is the critical heat flux (CHF) which marks the transition from the nucleate regime. At this point, a vapor layer begins forming over the heating surface, acting as an insulator. Consequently, the temperature of the cooled equipment can rise hundreds of degrees within a short period causing overheating or burnout [5,6]. To avoid the triggering of CHF, current pool boiling applications usually operate under a high safety factor, which means the benefit of nucleate boiling is not fully realized. Extensive research has been conducted to improve pool boiling heat transfer efficiency and reduce the risks of CHF, including surface modification [7], additives to coolants [8], enhancing fluid dynamics [9], and developing thermal management systems [10]. Among them, thermal management systems stand out for its real-time adjustments and versatile adaptability to diverse scenarios, which can prevent CHF while ensuring the cooling process operates within its maximum efficiency range. These features make thermal management particularly advantageous in handling transient conditions and heat load fluctuations. To realize the full potential of thermal management systems, accurate monitoring of the boiling process is essential, as it underpins the system's ability to respond effectively to dynamic boiling states. Traditional

boiling monitoring methods (e.g. thermocouples, thermistors) are intrusive which can lead to interference with boiling dynamics and lead to replacement difficulties. Nonintrusive methods (e.g. optical and acoustic) have been explored for analyzing and monitoring boiling.

Boiling image data has been shown to encode heat transfer information. McHale and Garimella [11] found heat flux correlations from physical descriptors (e.g. bubble departure diameter, void fraction) extracted from optical images. The introduction of machine learning and computer vision techniques have aided the speed and complexity of analysis. It has led to the utilization of optical data for various boiling monitoring tasks such as CHF detection. Hobold and Silva [12] reported that dimensionality reduction of bubble images using principal component analysis (PCA) allows the extracted principal components to be effectively utilized by support vector machine (SVM) and multilayer perceptron (MLP) classifiers for distinguishing between natural convection, nucleate boiling, and film boiling states. Hobold and Silva [13], then, proposed using Bayesian statistics to further improve the accuracy of film boiling detection based on convolutional neural networks (CNNs) and boiling images. To improve model generalizability, Al-Hindawi et al. [14] developed a GAN-based domain adaption framework for improving regime classification accuracy on cross-domain image datasets.

In addition to these cases where boiling images are used for classification/detection, they are also commonly employed to map heat flux. For instance, Hobold and Silva [15] used pool boiling images and machine learning models (e.g. MLP and CNN) to develop a real-time heat flux prediction module. Suh et al. [16] used CNN to extract abstract features from images, combined them with physical features of bubbles (e.g. bubble size, count) extracted using Mask R-CNN, to predict heat flux. They demonstrated that the inclusion of physical features led to model improvement. Dunlap et al. [17] developed several models for monitoring heat flux using image sequences and demonstrated that the PCA-CNN model achieves the best performance. Despite the widespread use of boiling images in experimental studies, their practical application faces several limitations. First, acquiring optical images imposes strict requirements on the experimental environment, such as lighting conditions, viewing angles, and background interference. Second, under high heat flux or intense boiling conditions, multiple bubbles may overlap or occlude each other, making feature extraction challenging and reducing detection accuracy. Additionally, the processes of bubble formation, growth, and collapse during boiling are very rapid, making it difficult to capture the full dynamics using static images or low-frame-rate videos. High-quality high-speed cameras are required to overcome this limitation; however, these devices are expensive and prone to damage in harsh environments, such as those with high temperatures and humidity. Therefore, the challenges faced by optical imaging in boiling monitoring highlight acoustic monitoring as a superior alternative.

Acoustic monitoring has more recently emerged as an approach for boiling understanding. In addition to offering a new perspective on boiling, it is compact, non-intrusive, lightweight, and cost-effective,

making it a more practical option for potential industrial applications. Hydrophones, acoustic emission (AE) sensors, and microphones [18–20] all belong to this category. Hydrophones have been used for uncovering boiling acoustic characteristics [21]. Tang et al. [22] used Fourier transform and wavelet transform to analyze boiling acoustic frequency and boiling modes. They found key takeaways such as the boiling sound intensity in microbubble emission boiling was significantly higher than other modes. Sinha et al. [23] used hydrophone and optical data to study boiling under different subcooling conditions, identifying distinct peak frequencies for the nucleate boiling regime and a unique explosive boiling mode. Hydrophone data has also been used for CHF detection. Sinha et al. [24] identified a peak frequency shift at the boiling crisis and then later developed a CNN [25] using hydrophone spectrograms to classify boiling regimes, enabling an advanced prediction system to power down and prevent CHF. Ueki and Ara [26] developed a classification model based on hydrophone data to distinguish boiling state transitions. Their proof of concept shows the possibility of monitoring systems via acoustic signals. Dunlap et al. [27] demonstrated the feasibility of using hydrophone data for acoustic heat flux monitoring but was limited by a small dataset. Ono et al. [28] used hydrophone frequency and cepstrum data with classification and regression models to predict microbubble emission boiling heat flux, finding cepstrum data to be more accurate and noise resistant.

While hydrophones are non-intrusive to the heater, they still need to be submerged in the liquid pool, which presents practical limitations. In contrast, AE sensors offer non-intrusive sensing by being mounted externally to the setup, recording acoustics from solid materials. However, AE sensors are high frequency sensors and due to the high sampling rates not all the data is saved. Instead, shorter waveforms or features are extracted from detected hits are stored. This data type will be further described in the next section. Several fields have adopted transient sampling methods for fault detection and system monitoring. Signals from AE sensors are used for rail system fault detection [29], crack growth prediction [30], pipe leak detection [31] and predicting the useful life of materials [32]. They have also been used in boiling research to analyze the acoustic characteristics of boiling [33,34]. Lim and Bang [34] provided an in-depth study on boiling AE acoustics, where they determined the mechanism for signal generation in boiling and found that the AE hit count correlated to heat flux. Baek et al. [35] compared boiling at 1 bar and 130 bar via AE signals and found differences in frequency ranges, AE energy, etc. Alhashan et al. [36] demonstrated the use of AE sensors for condition monitoring of the boiling bubbles. They found that specific AE parameters (e.g. amplitude, rise time, etc.) encode information about the occurrence and propagation of the bubbles. Other fields have adopted AE sensing for fault detection and system monitoring. Signals from AE sensors are used for detecting pipe leakage [37], gearbox fault detection [38,39], or predicting the useful life of materials [32]. However, to the best of our knowledge, AE has not yet been applied for heat flux prediction.

The primary challenges preventing AE data from being used for heat flux prediction lie in its low signal-to-noise ratio, the intrinsic discontinuity of AE hits, and limited dataset availability. To address these issues, we propose Hit2Flux, a novel approach that departs from traditional signal-to-heat flux point prediction methods. Leveraging a sequence-to-sequence architecture, our method can effectively capture the temporal dependencies between AE waveforms and heat flux variations while addressing the discontinuity of AE hits. This innovative solution enables accurate and robust heat flux monitoring under complex boiling conditions. Compared to conventional methods with thermistors, optical images, or hydrophones, our approach offers non-intrusive monitoring with superior application potential, making it a promising advancement for industrial and experimental boiling heat flux prediction. Additionally, since transient sampling from AE sensors is not unique to boiling applications, the Hit2Flux framework could easily be applied to other important areas of research and development.

The remainder of this paper is organized as follows: Section 2 provides a detailed description of the experimental setup, signal acquisition, data preprocessing, and the Hit2Flux model. Section 3 presents the testing results along with a corresponding discussion. The conclusions are summarized in Section 4.

2. METHODOLOGY

This section provides a detailed description of the experimental setup and the data collection. The data preprocessing and comprehensive structure of the machine learning model are also presented.

2.1 Experimental Setup

The experimental setup shown in Figure 1(a) consists of a stainless-steel boiling tank with two windows on the front and back. The windowpane has Pyrex glass within the inbuilt aluminum housing. The boiling tank is filled with deionized water. Two immersion heaters are used to reach and maintain the saturated liquid pool. A copper block with a CNC machined microchannel top surface is used as a boiling surface with an exposed surface area of 1 cm² submerged in deionized water. Four T-type thermocouples (Omega Engineering TJ36-CPSS-032U-6) with a 10kHz sampling rate are mounted alternatively at the side of the copper block in equally spaced intervals of 0.1 inch. These were used to approximate the surface temperature and heat flux at the surface using quasi-steady linear regression. Nine cartridge heaters (Omega Engineering HDC19102) were used to heat the copper block. The copper block was provided with ramp-up heating from 0 to CHF where the latter was determined by the temperature spikes. After the initiation of the CHF, the input power supply was turned off within 3 seconds to prevent unwanted thermal crises. A hydrophone (High Tech HTI-96 Min) with a 10,240 Hz sampling rate is submerged in the tank. An AE sensor (MISTRAS R3a) with a 1MHz sampling rate is mounted on the bottom of the tank and connected with a 1283 AE Node for data collection. The hydrophone is connected to a sound and vibration module

(NI 9230), while the thermocouples are interfaced with a temperature module (NI 9210). LabVIEW is used to save the data obtained from NI DAQ chassis (cDAQ-9178) for further processing. AEwin software is used to record and analyze the collected AE data.

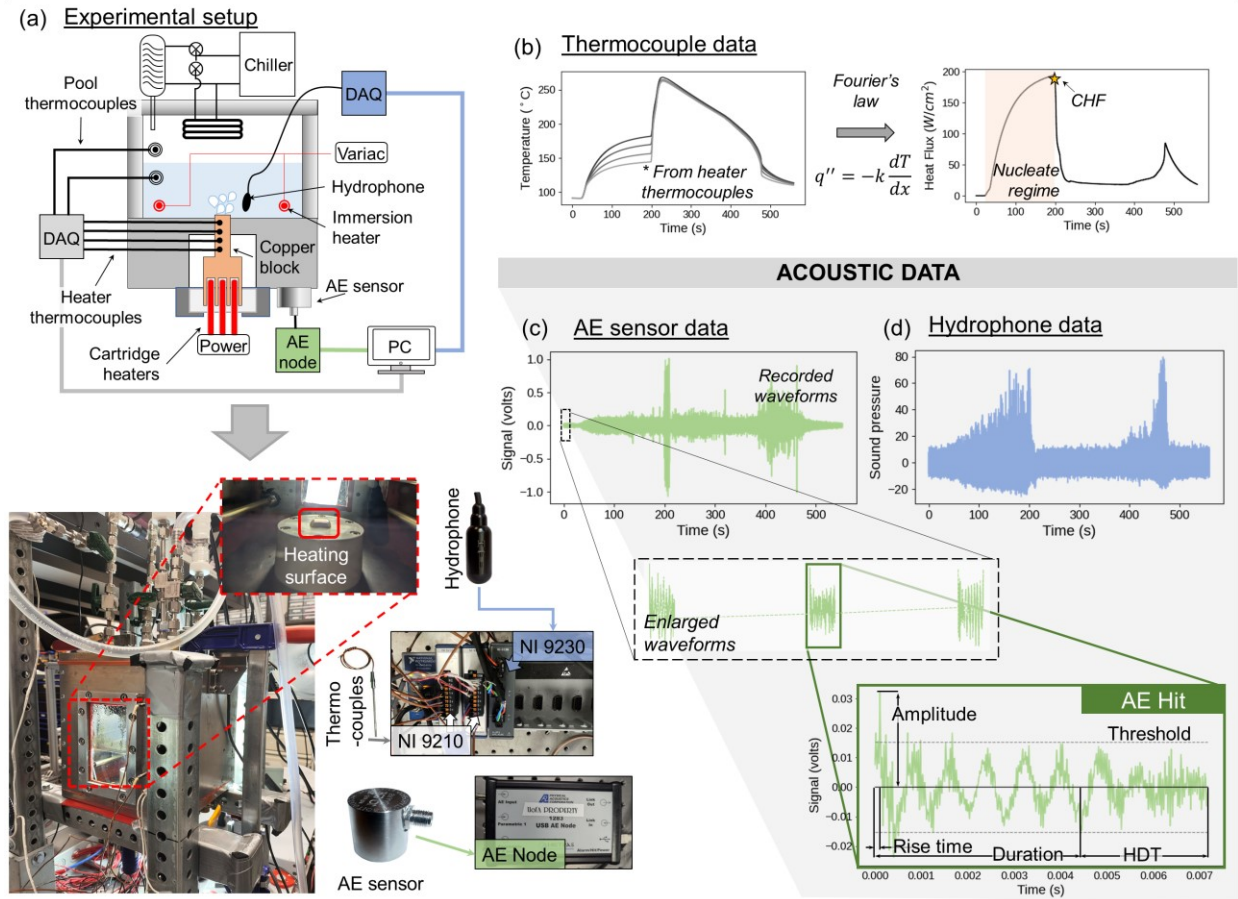


Figure 1. (a) Experimental setup schematic consisting of acoustic sensors (i.e., AE sensor and hydrophone). Data from a single transient experiment consisting of: (b) Thermocouple readings along copper block and calculated surface heat flux, (c) Recorded AE sensor data and hit feature definitions, and (d) recorded hydrophone data.

The setup employs two types of acoustic sensors: a hydrophone and an AE sensor. The hydrophone measures pressure variations from underwater sound waves, providing continuous voltage readings throughout the experiment. The recorded hydrophone data for one experiment is shown in Figure 1(d). In contrast, AE sensors detect high-frequency acoustic emissions in solids, but their data cannot be continuously recorded, as shown in Figure 1(c). Instead, for AE, only signals exceeding a user-defined threshold are saved to suppress white noise. For these experiments, a threshold of 45 dB was applied. An AE hit starts when the signal passes the threshold and lasts until the signal does not cross the threshold for a specified amount of time (i.e., hit definition time, HDT). From each AE hit, the amplitude is defined as

the highest absolute value signal reading during a hit. The rise time is defined as the amount of time from the first threshold passing to the amplitude. The count is defined as the number of times the signal passes the threshold during a hit. The duration is defined as the amount of time from the first threshold passing to the last in a hit [40]. For each hit, a waveform of length 7410 samples was saved from the AEWin software. Note, based on the characteristics of AE acquisition, a real hit may exceed the length of the saved waveform.

The heat flux data are obtained by Fourier's law. Specifically, taking the direction vertically upward from the lowest heater thermocouple as the positive direction, the positions of the four thermocouples are $[z_1, z_2, z_3, z_4]$, and their temperature readings $[T_1, T_2, T_3, T_4]$. The heat flux q of the copper foam surface is extrapolated by:

$$q = -k \cdot \frac{n \sum_{i=1}^n z_i T_i - (\sum_{i=1}^n z_i)(\sum_{i=1}^n T_i)}{n \sum_{i=1}^n z_i^2 - (\sum_{i=1}^n z_i)^2}, \quad (n = 4) \quad (1)$$

Where k is the thermal conductivity, in this experiment $k = 392W/(m \cdot K)$. Figure 1(b) provides an example of the temperature readings and the computed heat flux for one transient experiment. The heat flux data are used to create input-label pairs.

2.2 Data Preparation

An overview of the data preparation is shown in Figure 2. One boiling experiment consists of a sequence of the calculated heat fluxes $[q(t'_1), q(t'_2), \dots]$ and AE sensor hit waveforms $[H_1, H_2, H_3, \dots, H_m]$. Where each $H_i = [s(t_{i,1}), s(t_{i,2}), \dots, s(t_{i,Wl})]$ is the recorded waveform that starts at time $t_{i,1}$ and Wl is the recorded waveform length previously defined as 7410. The temporal spacing between each hit is not constant. From our past work [27], it was found that converting acoustic signal from the time domain to the frequency domain using fast Fourier transform (FFT) significantly improved the model performance. Therefore, in this work the FFT is used to convert each AE waveform (hit) into a vector of frequency intensities. To prepare the data, first each hit waveform is converted to the frequency domain using FFT $[H'_1, H'_2, \dots, H'_m]$. Where each frequency intensity vector H'_i is of length $Fl = Wl/2$. Using linear interpolation, the approximate heat flux at same time as the end of the recorded waveform was matched to each AE hit recorded waveform $[q(t_{1,Wl}), q(t_{2,Wl}), \dots, q(t_{m,Wl})]$. Additionally, our previous work [27] revealed that increasing the temporal coverage of a sample generally improves the performance of the heat flux regression model. With this knowledge, datasets with samples covering different temporal lengths were generated from the AE data. However, AE data presents greater complexity compared to hydrophone data. As AE data is sparse and consists of short 7.4 ms waveforms for each AE hit, addressing the challenge of extending the temporal coverage of model inputs becomes essential. To account for this, a rolling sampling method with window length N and stride α was used to generate hit sequences. The hit sequences can be given as $\{[H'_1, H'_2, \dots, H'_N], [H'_{1+\alpha}, H'_{2+\alpha}, \dots, H'_{N+\alpha}], \dots\}$. Essentially forming sequences-of-sequences

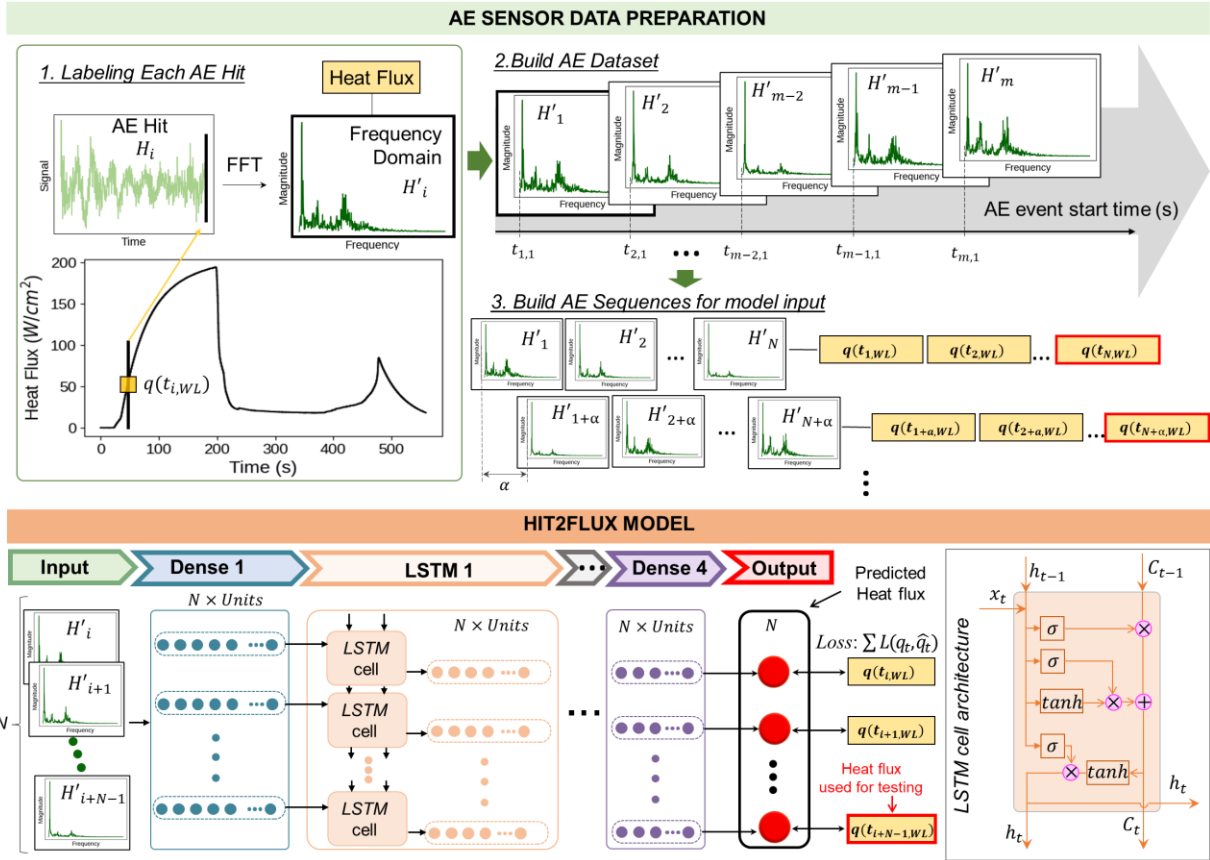


Figure 2. (Top panel) Data preparation method consisting of 1.) labeling each AE hit with a heat flux and converting to frequency domain, 2.) performing this operation for all hits in the dataset, and 3.) utilizing a rolling sampling technique to generate model inputs and outputs. (Bottom panel) Hit2Flux model architecture which takes inputs of hit frequencies and outputs heat flux sequences.

as inputs. Each sequence was matched to a corresponding sequence of heat fluxes $\{[q(t_{1, WL}), q(t_{2, WL}), \dots, q(t_{N, WL})], [q(t_{1+\alpha, WL}), q(t_{2+\alpha, WL}), \dots, q(t_{N+\alpha, WL})], \dots\}$ to be used for training the sequence-to-sequence models. Additionally, each hit sequence was matched the heat flux corresponding to the last hit in each sequence $[q(t_{N, WL}), q(t_{N+\alpha, WL}), \dots]$. These heat fluxes are used for testing the models and evaluation metric calculations. Data from four different boiling experiments were prepared in this way. Data prepared from 3 of the experiments were shuffled and split for use in both training and validation. Data from the other experiment was withheld for testing.

Hydrophone data was used for comparison on heat flux prediction performance. The hydrophone data was broken into short non-overlapping audio clips with the same temporal length as the recorded AE waveforms. They covered the same amount of time as the AE waveforms but contained fewer samples due to the smaller sampling rate of the hydrophones. After generating these clips, the same data preparation as the AE data shown in the top panel of Figure 2 is used. Each of these clips were transformed to the frequency domain with FFT and matched to a heat flux corresponding to same time as the last sample of the clip. The

length of the frequency vectors is $L_{HP} = 37$. Then, a rolling sampling method was used to generate hydrophone clip and heat flux sequences of length N . The hydrophone frequency vectors are used to train

Table 1. The architecture of the proposed Hit2Flux model.

Layer	Neurons/Units	Activation Function	Additional Parameters
Input	-	-	shape=(N,freq_len)
Dense	3000	Relu	-
LSTM	2000	-	return_sequences=True
Dropout	-	-	rate=0.2
LSTM	1000	-	return_sequences=True
LSTM	500	-	return_sequences=True
Dropout	-	-	rate=0.2
Dense	2000	Relu	-
Dropout	-	-	rate=0.2
Dense	1000	Relu	-
Dense	600	Relu	-
Dropout	-	-	rate=0.2
Dense	1	Linear	-

and test the same network used for AE. Additionally, the hydrophone data was also prepared based on our best performance model from our past work [27]. The comparison results and discussion will be provided in the following section.

2.3 Machine Learning Models

The developed Hit2Flux model is a sequence-to-sequence long short-term memory (LSTM) network for heat flux prediction, incorporating dense and dropout layers alongside the LSTM layers, as detailed in Table 1. The model explanation is provided as follows.

1) *Dense layer*. The Dense layer, also known as a fully connected layer, is a fundamental building block of neural networks. In this layer, each neuron is fully connected to all neurons in the previous layer or directly to the input data if it serves as the network's first layer. Each layer's operation consists of a linear transformation followed by a nonlinear activation function. Mathematically, consider an input consisting of N frequency vectors, each denoted as H'_i with a length of Fl (as previously defined). These vectors form an input matrix \mathbf{H}' of shape (N, Fl) . When this input passes through a dense layer with l neurons, the output \mathbf{H}'' is computed as $\mathbf{H}'' = \sigma(\mathbf{H}'W + b)$. Here, W is the weight matrix with shape (Fl, l) , b is the bias vector (broadcasted across rows) with shape $(l,)$, σ is the activation function, and \mathbf{H}'' is the output matrix with shape (N, l) . ReLU is a common activation function defined as $\sigma(x) = \max(0, x)$ and is used in several of the dense layers. These dense layers perform a similar operation for inputs from any preceding layer.

2) *LSTM layer*. Unlike dense layers, which transmit information in only one direction, LSTM layer incorporates gating mechanisms equipped with recurrent connections between its output and input, forming a feedback loop. These gated recurrent connections enable LSTM layer to feed their outputs back into their next input, allowing the network to remember and utilize information over time. As shown in the LSTM

cell architecture in figure 2, There are three gates in the LSTM cell, i.e., forget gate, input gate, and output gate. The cell receives two factors from last operation, i.e., h_{t-1} and C_{t-1} . h_{t-1} is the cell output for the input x_{t-1} . C_{t-1} is the cell state when input is x_{t-1} . With the current input vector x_t , the forget gate determines which information from the cell state should be discarded via a sigmoid operation. The computing equation are shown below:

$$f_t = \sigma(W_f[h_{t-1}, x_t] + b_f) \quad (2)$$

Where the $[\sim]$ operator is concatenating, W_f is the weight matrix with shape $(p, p + k)$ when the shape of h_{t-1} is p (p is the defined number of units in the LSTM) and shape of x_t is k , b_f is the bias vector with shape (p) , σ is the sigmoid activation function, and f_t is the output of forget gate also has shape (p) . The input gate regulates the incorporation of new information into the cell state, deciding what data should be added and updated. The operation including two parts choose information and create new cell state candidate. The computing equation are shown below:

$$i_t = \sigma(W_i[h_{t-1}, x_t] + b_i) \quad (3)$$

$$\hat{C}_t = \tanh(W_c[h_{t-1}, x_t] + b_c) \quad (4)$$

Where the W_* is the weight matrix, b_* is the bias vector, \tanh is the hyperbolic tangent function. After the operation of forget gate and input gate, the current cell state can update as

$$C_t = f_t \times C_{t-1} + i_t \times \hat{C}_t \quad (5)$$

The output gate controls what information the cell output based on the current input x_t , last output h_{t-1} , and the current cell state C_t . The computing equation of current output h_t are provide below:

$$h_t = \sigma(W_o[h_{t-1}, x_t] + b_o) \times \tanh(C_t) \quad (6)$$

For the next feature vector x_{t+1} , the LSTM layer repeat the above-mentioned procedure to extract the deep feature with temporal dependence.

3) *Dropout layer*. Dropout layers are used during training to reduce overfitting. They work by randomly deactivating a fraction of neurons, preventing them from contributing to both the outputs computation during forward propagation and the gradient update during backpropagation.

In general, a supervised regression model works by first initializing the model architecture and randomizing the weights and biases. Then, inputs and labels are provided for training. Inputs are passed through the model and compared to the labels using a loss function. Using backpropagation with the loss function, weights and biases are updated to minimize the loss. The process is repeated for a certain number of epochs until the loss convergences.

In this work, model was trained with an Adam optimizer and mean absolute error loss function L_{MAE} .

$$L = \frac{1}{A \times N} \sum_{j=1}^A \sum_{i=1}^N |q_{i,j} - \hat{q}_{i,j}| \quad (7)$$

Where A is the total number of sequences, N is the length of each sequence, $q_{i,j}$ is the true heat flux value, and $\widehat{q}_{i,j}$ is the predicted heat flux value. The model was set to run for 1000 epochs. Early stopping was used to stop the training process after 100 epochs of the validation loss not decreasing. The model weights at the epoch with the lowest validation loss were stored and used for testing. The model predicts a heat flux sequence of length N . To make comparisons, the last heat flux in the sequence was taken as the models output for testing. This operation ensures each model has the same number outputs regardless of the input sequence length. This model was built and trained in python using the TensorFlow library.

3. RESULTS & DISCUSSION

In this section, the acoustic signal collected by the AE sensor during the testing transient pool boiling experiment is used to test the effectiveness of the proposed Hit2Flux model. Moreover, to illustrate the superiority of Hit2Flux in heat flux prediction, the prediction results are also compared with different machine learning models, signal input types, and signal preprocessing methods.

3.1 Hit2Flux Model

Several models using the Hit2Flux architecture as previously described were trained and tested using AE sequences of varying lengths to evaluate whether samples spanning longer durations yield higher prediction accuracy. The sequence lengths N considered were 3, 5, 10, 15, 20, and 25 AE hits. Figure 3

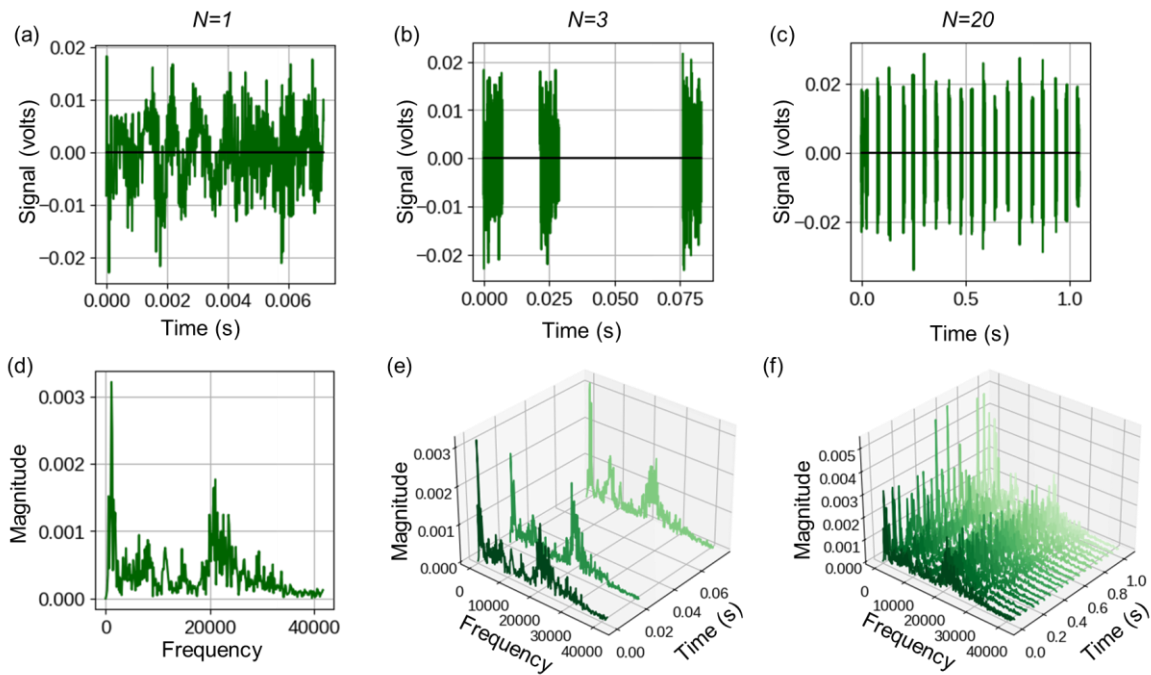


Figure 3. The raw AE signals and their frequency spectrum. (a) An AE waveform with its spectrum at (d). (b) An AE sequence with three AE hits and its spectrum at (e). (c) An AE sequence with twenty AE hits and its spectrum at (f).

shows some sequence examples with $N = 1, 3, 20$ where (a)~(c) are the raw AE waveforms, (d)~(f) are their frequency spectrum. Figure 3(a) highlights the high-frequency and short-duration characteristics of an AE waveform, while (b) and (c) demonstrate the discontinuity of the waveforms. These characteristics make direct heat flux prediction using AE waveform more challenging compared to the continuous natured hydrophone acoustics. Consequently, most studies on boiling AE have focused on exploring AE characteristics during the boiling process or analyzing changes in AE features at key moments, rather than heat flux monitoring. In contrast, this work introduces the "sequences of sequences" approach, enabling the effective utilization of AE waveforms for heat flux prediction. Based on the raw AE sequences, the FFT is applied to transfer them to frequency domain as shown in (d) to (f). These frequency vectors are feed into the proposed Hit2Flux model.

Figure 4 provides the comparison results of the predicted heat flux values against the true heat flux labels for the testing data. Ideally, each point would follow the diagonal black line which means each predicted heat flux is the same as the true heat flux label. It can be seen that, in general, as the sequence length increases the heat flux predictions improve. Since the points get less sparse and more closely follow the diagonal line. Figure 4(f) shows the best fit of the AE sequences, corresponding to an input sequence length of 25 AE hits.

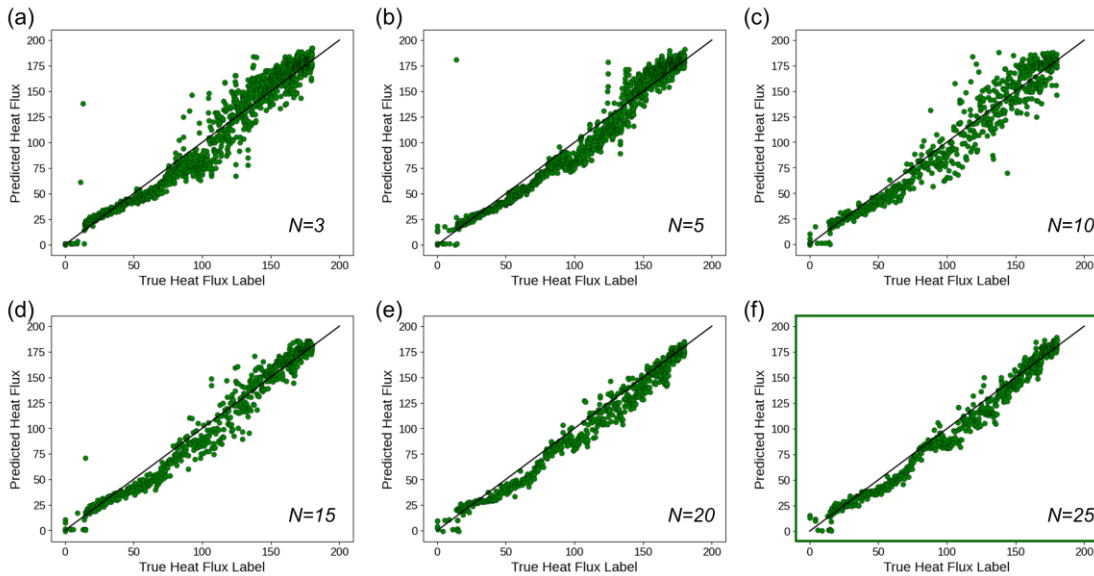


Figure 4. The testing results with different input sequence length N . (a) $N=3$. (b) $N=5$. (c) $N=10$. (d) $N=15$; (e) $N=20$. (f) $N=25$.

To quantitatively compare the performance with different sequence lengths two metrics were used; coefficient of performance (R^2) and mean squared error (MSE). Their calculation equations are given below:

$$R^2 = 1 - \frac{\sum_{i=1}^A (q_i - \hat{q}_i)^2}{\sum_{i=1}^A (q_i - \bar{q})^2} \quad (8)$$

$$MSE = \frac{1}{A} \sum_{i=1}^A (q_i - \hat{q}_i)^2 \quad (9)$$

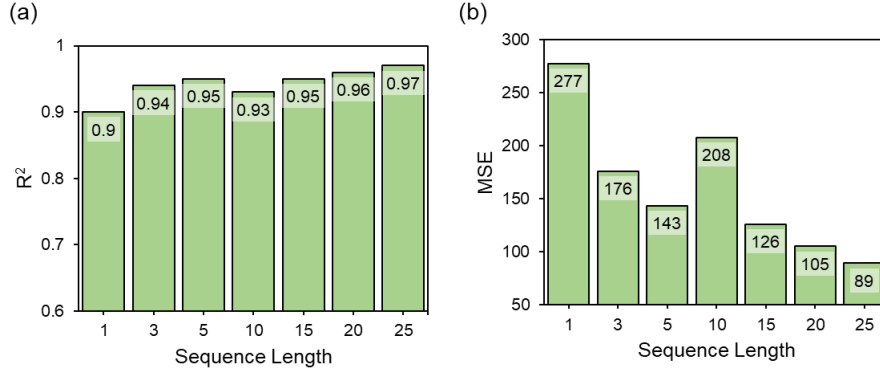


Figure 5. Quantitative results of the proposed method with varying input sequence lengths. (a) The R^2 scores. (b) The mean squared errors. It demonstrates the effectiveness of the Hit2Flux model and highlights the relationship between model performance and input AE sequence length, showing that longer sequences result in improved performance.

The R^2 score is a value in the range from 0 to 1 which demonstrates how well a model fits the data. A higher R^2 value indicates a better fit. The MSE is a measure of the spread of the data points around the mean. The smaller the MSE the more densely clustered around the mean. Based on these metrics the best model will be the one with the highest R^2 and lowest MSE. Figure 5(a) is a bar plot of R^2 scores for the different sequence lengths and Figure 5(b) is a bar plot of the different MSE values for the sequence lengths. Similar to the visual comparison conclusion from Figure 4, the model trained with 25 AE hits sequence length performs the best; it achieved an R^2 value of 0.97 and a MSE of 89. It is also seen that in general as the sequence length increases these metrics both improve. These results also demonstrate that the Hit2Flux model can effectively monitor boiling heat flux using data from AE sensors.

3.2 Methods Comparison

The core characteristic of the proposed method lay on the data organization, signal processing, and the developed model. It can be summarized as AE+FFT+sequences-of-sequences-input+sequence-to-sequence-LSTM. To further validate the superiority of the proposed method, several different methods with different signal processing and state-of-arts model combination are used here for comparison. The raw signal, spectrum, cepstrum, and AE features (i.e., hit, amplitude, count, etc.) are paired with Multilayer perceptron (MLP), Random Forest Regression (RFR), Gaussian Process Regression (GPR), Convolutional neural network (CNN), and LSTM. Only combinations that obtained R^2 values above 0.1 are reported. Table 2 summarizes the performance evaluation results on the AE signals. MLP has the best result with R^2

Table 2. Performance summarization of models with different combinations of methods, feature extractions, and sequence lengths.

Method	Feature Extraction	Hits Per Input (N)	R2	MSE	
MLP	-	1	0.68	901	
		25	0.12	2350	
	Spectrum	1	0.89	308	
		25	0.94	161	
	Cepstrum	25	0.6	1083	
RFR	AE Features	1	0.71	818	
		25	0.69	809	
GPR	Spectrum	1	0.82	518	
	Cepstrum	1	0.77	665	
CNN	-	1	0.52	1357	
		25	0.71	766	
	Spectrum	1	0.89	327	
		25	0.95	142	
	Cepstrum	1	0.69	878	
		25	0.89	280	
	LSTM (Ours)	-	25	0.84	406
		Spectrum	25	0.97	89
Cepstrum		25	0.95	126	

of 0.94 when FFT is applied and sequence length is 25. Among all the feature types, AE features only works well when and RFR model is used. GPR is functional when the input consists of a single hit and the spectrum or cepstrum is used as the input representation. However, its best R2 and MSE are only 0.82 and 518 respectively. CNN works for the raw signal, spectrum, or cepstrum inputs. The CNN+Spectrum+25-sequence achieves the best performance with 0.95 of R2 and 142 of MSE. This result indicates the effectiveness of FFT and sequence input. However, when compare with the LSTM model, other methods are far inferior. The LSTM+Spectrum+25-sequence achieves the highest R2 at 0.97 and lowest MSE at 89. At the same hit sequence length, LSTM performs better when using the spectrum obtained via FFT as input compared to using the raw signal or cepstrum as input. In summary, the highest R2 score and the lowest MSE values proves the superiority of the proposed Hit2Flux model. It also highlights the importance of FFT, the sequences-of-sequences-input, and the temporal information extraction for heat flux prediction.

3.3 Hydrophone Data Comparison

Comparative tests were also conducted between AE signals and hydrophone signals. Principal component analysis (PCA) was applied to extract the first principal component (PC-1) from the raw AE and hydrophone signals. The distribution of PC-1 at different heat flux levels is presented in Figure 6. The figure shows that AE signals exhibit broader variance in PC-1, whereas hydrophone signals display a more concentrated distribution. This difference suggests that AE signals have higher variability compared to hydrophone signals, particularly in the high heat flux stage. This increased variability indicates that AE

signals are more susceptible to high-energy transient events, making heat flux prediction from AE signals more challenging.

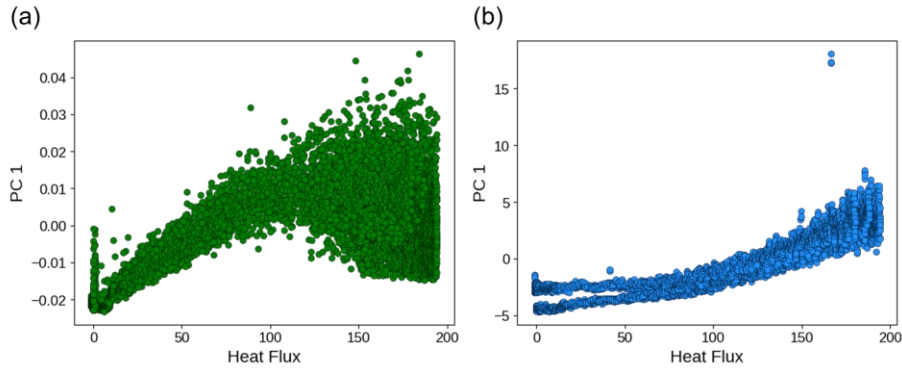


Figure 6. The comparison of first principal component (PC-1) at different heat flux. (a) The PC-1 of raw AE signal. (b) The PC-1 of raw hydrophone signal.

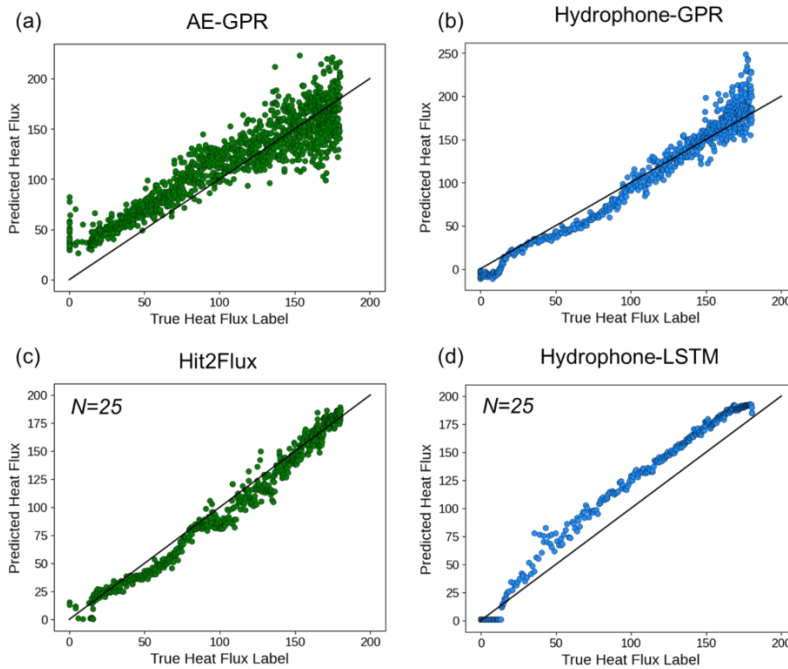


Figure 7. The heat flux prediction results of AE and Hydrophone as inputs. (a) AE input with GPR model. (b) Hydrophone input with GPR model. (c) AE input with the proposed model. (d) Hydrophone input with the proposed model.

Our past work [27] found the FFT-GPR model to be superior for hydrophone heat flux prediction. Therefore, GPR models were developed using the raw AE and hydrophone data to compare their performance in heat flux prediction. The comparison results, as shown in Figure 7 (a) and (b), indicate that hydrophone data outperform AE data as inputs. These findings also align with the observations in Figure 6 where the PC-1 of AE signals are unstable compared to hydrophone signals, making heat flux prediction more challenging when using AE signal as input for classic regression model. However, when using the proposed method, the situation is different. As shown in Figure 7 (c) and (d), the AE signal input for the

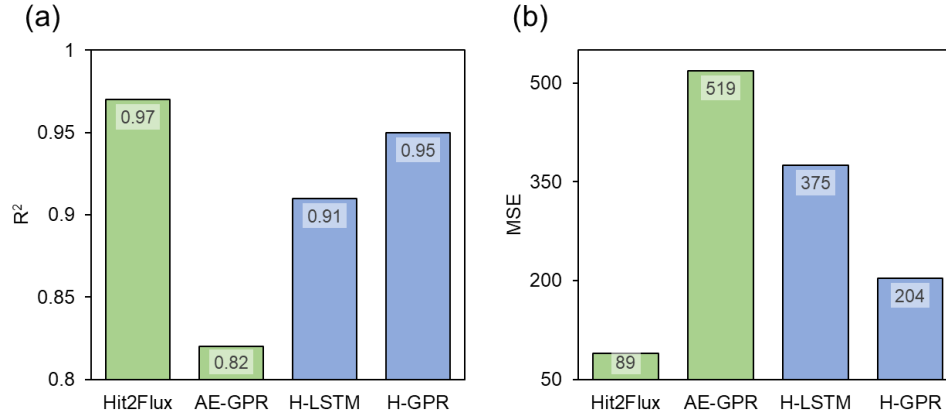


Figure 8. The qualitative results of comparison. (a) R² score of all the inputs and models. (b) MSE of all the inputs and models.

proposed model have more concentrated distribution compare to hydrophone especially as the heat flux increases. All the qualitative results are provided in Figure 8, which shows that the Hit2Flux model has a R² score of 0.97 and a MSE at 89 where the hydrophone has lower R² score at 0.88 and higher MSE at 519. These results indicate that the proposed model exhibits superior noise suppression and feature extraction capabilities. It can also be inferred that AE signals carry more information due to their significantly higher sampling rate. This is particularly evident in the high heat flux regime, where predictions based on AE signals exhibit a more consistent distribution, reflecting the characteristics of AE data collection. As boiling becomes more intense, AE signals are more likely to exceed the threshold and be recorded. Consequently, within the same time frame, AE signals capture more critical information compared to hydrophone signals.

4. CONCLUSION

In this paper, we propose a novel method for predicting transient pool boiling heat flux with a non-intrusive sensor. The proposed method uses acoustics acquired by AE sensor as the driven data, i.e., AE hits (waveforms). Firstly, the AE hits are organized in sequence to form the sequences of sequences pattern. Then, the fast Fourier transform is employed to transfer the time domain data to frequency domain. Further, the frequency sequences are input to the proposed Hit2Flux model for heat flux monitoring. Transient pool boiling experiments were conducted to collect data, and the proposed method was validated using the acquired signals with varying sequence lengths. Additionally, the method was compared with hydrophone-based heat flux prediction and several other approaches utilizing AE signals. Experimental results demonstrate that the proposed method offers significantly higher accuracy compared to existing approaches. Based on the experimental findings, the following conclusions can be drawn: i) Data from the non-intrusive AE sensor can successfully be used for heat flux prediction. As seen by the best model achieving a high R² of 0.97 and relatively low MSE of 89. ii) Input sequences of AE hit waveform frequencies generate the best model performance. Additionally, the more hits included in an input sequence

are shown to improve the performance on test data. And iii) the best AE signal model outperformed the hydrophone-based predictions for the test data. Which demonstrates the improved generalizability of the Hit2Flux model compared to past work. Future work will focus on extending the boiling experiments to include variations in heater surfaces, operating pressures, and working fluids to further enhance the generalizability of the proposed method.

Acknowledgments

This study was supported by the National Science Foundation under Grant No. CBET-2323022.

REFERENCES

- [1] H. Li, Z. Ju, Q. Li, X. Chen, Design and optimization of diamond-aluminum thermal spreading substrate for thermal management in high-power electronic devices, *Appl Therm Eng* (2025) 125662.
- [2] Y. Li, B. Kong, C. Qiu, Y. Li, Y. Jiang, Numerical study on air-cooled battery thermal management system considering the sheer altitude effect, *Appl Therm Eng* 258 (2025) 124707.
- [3] Q. Zhang, Z. Meng, X. Hong, Y. Zhan, J. Liu, J. Dong, T. Bai, J. Niu, M.J. Deen, A survey on data center cooling systems: Technology, power consumption modeling and control strategy optimization, *Journal of Systems Architecture* 119 (2021) 102253.
<https://doi.org/10.1016/J.SYSARC.2021.102253>.
- [4] X. Wu, J. Yang, Y. Liu, Y. Zhuang, S. Luo, Y. Yan, L. Xiao, X. Han, Investigations on heat dissipation performance and overall characteristics of two-phase liquid immersion cooling systems for data center, *Int J Heat Mass Transf* 239 (2025) 126575.
- [5] H. Pandey, C. Li, C. Dunlap, H. Hu, Unveiling hysteresis of transient boiling: A multimodal perspective, *Appl Therm Eng* 262 (2025) 125259.
- [6] S. Barathula, R. Kandasamy, P.J.Y. Fok, T.N. Wong, K.C. Leong, K. Srinivasan, Heat load prediction in flow boiling using boiling-induced vibrations aided with machine learning, *Int J Heat Mass Transf* 232 (2024) 125890.
- [7] S. Mori, Y. Utaka, Critical heat flux enhancement by surface modification in a saturated pool boiling: A review, *Int J Heat Mass Transf* 108 (2017) 2534–2557.
<https://doi.org/10.1016/J.IJHEATMASSTRANSFER.2017.01.090>.
- [8] G. Liang, I. Mudawar, Review of pool boiling enhancement with additives and nanofluids, *Int J Heat Mass Transf* 124 (2018) 423–453.
<https://doi.org/10.1016/J.IJHEATMASSTRANSFER.2018.03.046>.
- [9] A. Inbaoli, C.S. Sujith Kumar, S. Jayaraj, A review on techniques to alter the bubble dynamics in pool boiling, *Appl Therm Eng* 214 (2022) 118805.
<https://doi.org/10.1016/J.APPLTHERMALENG.2022.118805>.

- [10] C. Wu, Y. Sun, H. Tang, S. Zhang, W. Yuan, L. Zhu, Y. Tang, A review on the liquid cooling thermal management system of lithium-ion batteries, *Appl Energy* 375 (2024) 124173.
- [11] J.P. McHale, S. V. Garimella, Nucleate boiling from smooth and rough surfaces–Part 2: Analysis of surface roughness effects on nucleate boiling, *Exp Therm Fluid Sci* 44 (2013) 439–455.
- [12] G.M. Hobold, A.K. da Silva, Machine learning classification of boiling regimes with low speed, direct and indirect visualization, *Int J Heat Mass Transf* 125 (2018) 1296–1309. <https://doi.org/10.1016/J.IJHEATMASSTRANSFER.2018.04.156>.
- [13] G.M. Hobold, A.K. da Silva, Automatic detection of the onset of film boiling using convolutional neural networks and Bayesian statistics, *Int J Heat Mass Transf* 134 (2019) 262–270. <https://doi.org/10.1016/j.ijheatmasstransfer.2018.12.070>.
- [14] F. Al-Hindawi, T. Soori, H. Hu, M.M.R. Siddiquee, H. Yoon, T. Wu, Y. Sun, A framework for generalizing critical heat flux detection models using unsupervised image-to-image translation, *Expert Syst Appl* 227 (2023) 120265. <https://doi.org/10.1016/J.ESWA.2023.120265>.
- [15] G.M. Hobold, A.K. da Silva, Visualization-based nucleate boiling heat flux quantification using machine learning, *Int J Heat Mass Transf* 134 (2019) 511–520. <https://doi.org/10.1016/j.ijheatmasstransfer.2018.12.170>.
- [16] Y. Suh, R. Bostanabad, Y. Won, Deep learning predicts boiling heat transfer, *Sci Rep* 11 (2021) 1–11. <https://doi.org/10.1038/s41598-021-85150-4>.
- [17] C. Dunlap, C. Li, H. Pandey, Y. Sun, H. Hu, A Temporal-Spatial Framework for Efficient Heat Flux Monitoring of Transient Boiling, *IEEE Trans Instrum Meas* (2024).
- [18] K. Zhang, J. Yang, C. Huang, X. Huai, Nonintrusive identification of boiling regimes enabled by deep learning based on flow boiling acoustics, *Int J Heat Mass Transf* 236 (2025). <https://doi.org/10.1016/j.ijheatmasstransfer.2024.126290>.
- [19] S. Barathula, S.K. Chaitanya, K. Srinivasan, Evaluation of machine learning models in the classification of pool boiling regimes up to critical heat flux based on boiling acoustics, *Int J Heat Mass Transf* 201 (2023) 123623. <https://doi.org/10.1016/j.ijheatmasstransfer.2022.123623>.
- [20] I.C. Geraldo, T. Bose, K.M. Pekpe, J.P. Cassar, A.R. Mohanty, K. Paumel, Acoustic monitoring of sodium boiling in a liquid metal fast breeder reactor from autoregressive models, *Nuclear Engineering and Design* 278 (2014) 573–585. <https://doi.org/10.1016/j.nucengdes.2014.07.026>.
- [21] H. Nishihara, Y. Bessho, Acoustic emission in subcooled nucleate pool boiling, *J Nucl Sci Technol* 14 (1977) 407–415. <https://doi.org/10.1080/18811248.1977.9730779>.
- [22] J. Tang, G. Xie, J. Bao, Z. Mo, H. Liu, M. Du, Experimental study of sound emission in subcooled pool boiling on a small heating surface, *Chem Eng Sci* 188 (2018) 179–191. <https://doi.org/10.1016/j.ces.2018.05.002>.
- [23] K. Nishant Ranjan Sinha, D. Ranjan, N. Kumar, M. Qaisar Raza, R. Raj, Simultaneous audio-visual-thermal characterization of transition boiling regime, *Exp Therm Fluid Sci* 118 (2020). <https://doi.org/10.1016/j.expthermflusci.2020.110162>.

- [24] K. Nishant Ranjan Sinha, D. Ranjan, M.Q. Raza, N. Kumar, S. Kaner, A. Thakur, R. Raj, In-situ acoustic detection of critical heat flux for controlling thermal runaway in boiling systems, *Int J Heat Mass Transf* 138 (2019) 135–143. <https://doi.org/10.1016/j.ijheatmasstransfer.2019.04.029>.
- [25] K.N.R. Sinha, V. Kumar, N. Kumar, A. Thakur, R. Raj, Deep learning the sound of boiling for advance prediction of boiling crisis, *Cell Rep Phys Sci* 2 (2021).
- [26] Y. Ueki, K. Ara, Proof of concept of acoustic detection of boiling inception and state transition using deep neural network, *International Communications in Heat and Mass Transfer* 129 (2021). <https://doi.org/10.1016/j.icheatmasstransfer.2021.105675>.
- [27] C. Dunlap, H. Pandey, E. Weems, H. Hu, Nonintrusive Heat Flux Quantification Using Acoustic Emissions During Pool Boiling, *Appl Therm Eng* (2023) 120558. <https://doi.org/10.1016/j.applthermaleng.2023.120558>.
- [28] J. Ono, Y. Aoki, N. Unno, K. Yuki, K. Suzuki, Y. Ueki, S. ichi Satake, Acoustic state detection of microbubble emission boiling using a deep neural network based on cepstrum analysis, *International Journal of Multiphase Flow* 166 (2023). <https://doi.org/10.1016/j.ijmultiphaseflow.2023.104512>.
- [29] A. Pal, A.K. Datta, Development of Smart Real-time Fault Detection Approach in Railway Track Deploying a Single Acoustic Emission Sensor Data, *Journal of Vibration Engineering and Technologies* (2024). <https://doi.org/10.1007/s42417-024-01374-4>.
- [30] M. Chai, X. Hou, Z. Zhang, Q. Duan, Identification and prediction of fatigue crack growth under different stress ratios using acoustic emission data, *Int J Fatigue* 160 (2022). <https://doi.org/10.1016/j.ijfatigue.2022.106860>.
- [31] A. Rai, Z. Ahmad, M.J. Hasan, J.M. Kim, A novel pipeline leak detection technique based on acoustic emission features and two-sample kolmogorov–smirnov test, *Sensors* 21 (2021). <https://doi.org/10.3390/s21248247>.
- [32] T.K. Nguyen, Z. Ahmad, J.M. Kim, A scheme with acoustic emission hit removal for the remaining useful life prediction of concrete structures, *Sensors* 21 (2021). <https://doi.org/10.3390/s21227761>.
- [33] S. Bin Seo, I.C. Bang, Acoustic analysis on the dynamic motion of vapor-liquid interface for the identification of boiling regime and critical heat flux, *Int J Heat Mass Transf* 131 (2019) 1138–1146. <https://doi.org/10.1016/j.ijheatmasstransfer.2018.11.136>.
- [34] D.Y. Lim, I.C. Bang, A novel non-destructive acoustic approach for investigating pool boiling phenomena, *Int J Heat Mass Transf* 222 (2024) 125166.
- [35] S.H. Baek, K. Wu, H.S. Shim, D.H. Lee, J.G. Kim, D.H. Hur, Acoustic emission monitoring of water boiling on fuel cladding surface at 1 bar and 130 bar, *Measurement (Lond)* 109 (2017) 18–26. <https://doi.org/10.1016/j.measurement.2017.05.042>.
- [36] T. Alhashan, A. Addali, J. Amaral Teixeira, S. Elhashan, Identifying bubble occurrence during pool boiling employing acoustic emission technique, *Applied Acoustics* 132 (2018) 191–201. <https://doi.org/10.1016/j.apacoust.2017.11.006>.

- [37] S. Ahmad, Z. Ahmad, C.H. Kim, J.M. Kim, A Method for Pipeline Leak Detection Based on Acoustic Imaging and Deep Learning, *Sensors* 22 (2022). <https://doi.org/10.3390/s22041562>.
- [38] R. Li, S.U. Seçkiner, D. He, E. Bechhoefer, P. Menon, Gear fault location detection for split torque gearbox using AE sensors, *IEEE Transactions on Systems, Man and Cybernetics Part C: Applications and Reviews* 42 (2012) 1308–1317. <https://doi.org/10.1109/TSMCC.2011.2182609>.
- [39] L. Liu, L. Chen, Z. Wang, D. Liu, Early Fault Detection of Planetary Gearbox Based on Acoustic Emission and Improved Variational Mode Decomposition, *IEEE Sens J* 21 (2021) 1735–1745. <https://doi.org/10.1109/JSEN.2020.3015884>.
- [40] G. Ciaburro, G. Iannace, Machine-Learning-Based Methods for Acoustic Emission Testing: A Review, *Applied Sciences (Switzerland)* 12 (2022). <https://doi.org/10.3390/app122010476>.